Naval Research Laboratory

Washington, DC 20375-5320

NRL/MR/6040--17-9699

Pressure Characteristics of a Diffuser in a Ram-RDE Propulsive Device

Douglas A. Schwer
Kazhikathra Kailasanath

Laboratories for Computational Physics and Fluid Dynamics
Materials Science and Component Technology Directorate

Thomas Kaemming

Innovative Scientific Solutions Incorporated
Dayton, Ohio

July 21, 2017

REPORT DOCUMENTATION PAGE

Form Approved
OMB No. 0704-0188

1. REPORT DATE *(DD-MM-YYYY)*	**2. REPORT TYPE**	**3. DATES COVERED** *(From - To)*
21-07-2017	Memorandum Report	

4. TITLE AND SUBTITLE

Pressure Characteristics of a Diffuser in a Ram-RDE Propulsive Device

5a. CONTRACT NUMBER
64-4493-06

5b. GRANT NUMBER

5c. PROGRAM ELEMENT NUMBER

6. AUTHOR(S)

Douglas A. Schwer, Kazhikathra Kailasanath, and Thomas Kaemming[1]

5d. PROJECT NUMBER

5e. TASK NUMBER

5f. WORK UNIT NUMBER

7. PERFORMING ORGANIZATION NAME(S) AND ADDRESS(ES)

Naval Research Laboratory, Code 6041
Laboratories for Computational Physics and Fluid Dynamics
4555 Overlook Avenue, SW
Washington, DC 20375-5344

8. PERFORMING ORGANIZATION REPORT NUMBER

NRL/MR/6040--17-9699

9. SPONSORING / MONITORING AGENCY NAME(S) AND ADDRESS(ES)

Office of Naval Research
875 N. Randolph Street, Suite 1425
Arlington, VA 22203-1995

10. SPONSOR / MONITOR'S ACRONYM(S)

ONR

11. SPONSOR / MONITOR'S REPORT NUMBER(S)

12. DISTRIBUTION / AVAILABILITY STATEMENT

Approved for public release; distribution is unlimited.

13. SUPPLEMENTARY NOTES

[1]Innovative Scientific Solutions Incorporated, 7610 McEwen Road, Dayton, OH 45459

14. ABSTRACT

This report focuses on dynamic simulations of a representative ram RDE subsonic diffuser to study ram RDE compatibility with a supersonic inlet. Of particular interest is the propagation of pressure perturbations due to the detonation waves in the RDE combustion chamber. Simulations were completed using a notional diffuser for a ram RDE device operating at 42,000 ft and Mach 2.5. A previous RDE code was used to provide an exhaust forcing function assuming a slot injector plate. A total of 8 different exhaust forcing functions were used, representing RDE air-valve area ratios between 0.3 and 0.6 in single and dual shock operation. Simulations were then completed for the diffuser with the Propel code for each of these exhaust forcing functions. Analysis indicates that the amount of pressure variation seen near the inlet is very sensitive to the shape of the forcing function. The broad pressure rise of the lower area ratios tend to remain intact through the diffuser to the intake with minimal dissipation, while the sharper pressure peak of the higher area ratios tend to be dissipated to a larger degree. For single-shock operation, the amount of pressure variation at the intake varies from 20.5% (area ratio of 0.3) to 39.1% (a=0.6). Dual-shock operation further sharpens the peak of the forcing function. For dual-shock operation, the amount of pressure variation at the intake varies from 21.0% (a=0.3) to 21.9% (a=0.6) for the different area ratios.

15. SUBJECT TERMS

Air-breathing propulsion
Detonation
Continuous detonation
Rotating-detonation-engine
Ethylene-air
Diffuser
Pressure feedback
Modeling and simulation

16. SECURITY CLASSIFICATION OF:			**17. LIMITATION OF ABSTRACT**	**18. NUMBER OF PAGES**	**19a. NAME OF RESPONSIBLE PERSON**
a. REPORT	**b. ABSTRACT**	**c. THIS PAGE**			Douglas A. Schwer
Unclassified Unlimited	Unclassified Unlimited	Unclassified Unlimited	Unclassified Unlimited	22	**19b. TELEPHONE NUMBER** *(include area code)* (202) 767-3615

Standard Form 298 (Rev. 8-98)
Prescribed by ANSI Std. Z39.18

CONTENTS

EXECUTIVE SUMMARY

This report focuses on dynamic simulations of a representative ram RDE subsonic diffuser to study ram RDE compatibility with a supersonic inlet. Of particular interest is the propagation of pressure perturbations due to the detonation waves in the RDE combustion chamber. Simulations were completed using a notional diffuser for a ram RDE device operating at 42,000 ft and Mach 2.5. A previous RDE code was used to provide an exhaust forcing function assuming a slot injector plate. A total of 8 different exhaust forcing functions were used, representing RDE air-valve area ratios between 0.3 and 0.6 in single and dual shock operation. Simulations were then completed for the diffuser with the Propel code for each of these exhaust forcing functions. Analysis indicates that the amount of pressure variation seen near the inlet is very sensitive to the shape of the forcing function. The broad pressure rise of the lower area ratios tend to remain intact through the diffuser to the intake with minimal dissipation, while the sharper pressure peak of the higher area ratios tend to be dissipated to a larger degree. For single-shock operation, the amount of pressure variation at the intake varies from 20.5% (area ratio of 0.3) to 39.1% (a=0.6). Dual-shock operation further sharpens the peak of the forcing function. For dual-shock operation, the amount of pressure variation at the intake varies from 21.0% (a=0.3) to 21.9% (a=0.6) for the different area ratios.

PRESSURE CHARACTERISTICS OF A DIFFUSER IN A RAM-RDE PROPULSIVE DEVICE

INTRODUCTION

This report focuses on the diffuser of a ram Rotating Detonation Engine (RDE) device. A ram RDE is a ramjet with the constant pressure combustion chamber replaced with a Rotating Detonation Engine combustor to accomplish pressure gain combustion. A ram engine (whether jet or RDE) works by using the engine's forward motion to compress the incoming air without a compressor. This allows for a simplified design, and for moderate supersonic devices (Mach 2-3) is efficient enough to be competitive with other types of engine designs. Part of the attraction of using an RDE is its pressure gain, which offers improved thermodynamic efficiency and may extend its efficient operation to lower pressure ratios and Mach numbers. A notional ram RDE engine is shown in Figures 1 and 2. Note the center body that creates an annular combustion chamber for the RDE.

The supersonic inlet is not shown in either figure, but would be very similar to an inlet for a standard ramjet device. The supersonic inlet decelerates the flow with minimal losses to a low supersonic condition. The air is then processed through a normal shock resulting in subsonic flow, and the flow is further decelerated through the diffuser. For a ram RDE, some sort of a valve or isolator is required between the diffuser and combustion chamber to limit pressure oscillations propagating forward into the diffuser and disrupting the inlet flow. In previous numerical and experimental studies, this has typically been called the injection system, but for air-breathing engines it is more appropriate to call it an air valve or air inlet, and we will use these terms interchangeably. The fresh premixture is detonated near the air inlet and the hot product gases are expanded through the engine with an approximately constant cross-sectional area. Lastly, the product gases are exhausted through the propulsive convergent-divergent nozzle. The effect of the conical taper is to reduce the swirl generated by the oblique shock-wave [1,2]. The nozzle architecture for a ram RDE has not been completed yet, and may change substantially for a final design.

Thermodynamic stations are shown in Figure 2 for a ram RDE device. The stations follow the gas turbine specification given in [3]. Station 1 is positioned just ahead of the diffuser, after the supersonic flow has been decelerated to just over Mach 1. Station 1.2 is on the other side of the diffuser throat, after the gas has been processed by a normal shock wave at the diffuser throat. Since there is no compressor for a ram device, station 2 and 3 coincide. Station 3 is just ahead of the air valve, after the flow has been decelerated by the diffuser to moderate Mach numbers. Station 3* is an additional station required by an RDE that takes into account losses from the air inlet, after the fuel is mixed into the air flow but before the gases are processed by the detonation wave. Station 4 is the thermodynamic state for the hot product gases. Because of the nature of the RDE, there is no one condition at station 4, but a range of conditions. This is partly due to a range of pressure in the fill region. Also, the gases expand azimuthally and axially through the straight section of the RDE due to the strong multi-dimensional flow-field. The thermodynamic properties of detonation engines in general and RDEs specifically have been addressed in several other papers [4-8]. In those studies, state 4 represents the average CJ state. State 5 for gas turbines represents the outlet of the turbine, and has no meaning in this configuration. State 6 is the mixer (if the engine has bypass air) and afterburner, and for this configuration, also does not exist. States 7-9 represent the propulsive nozzle.

To date, considerable effort has gone into characterizing the RDE flow from the combustion chamber through the nozzle exhaust, but almost no attention has been given upstream of the combustion chamber. For this report, we are interested in pressure perturbations that flow upstream from the detonation wave into the diffuser. If the pressure perturbations are strong enough, they can disrupt the

Manuscript approved August 23, 2016.

shock wave at the throat of the diffuser and the supersonic inlet flow, and can cause either inlet unstart or cause the diffuser to swallow the shock wave. Both events are potentially serious conditions for operating a ram RDE. For this project, we have selected a "notional" geometry and conditions that represent conditions along a flight path for a ram RDE. The focus of the paper will be on the pressure and flow perturbations that are seen at the throat of the diffuser for different RDEs based on the air-valve area ratio.

GEOMETRY AND CONDITIONS

The engine and diffuser lines are representative of a supersonic tactical missile. The outer diameter of the combustion chamber is 12 inches (304.8 mm), and the inside diameter is 8.4 inches (213.4 mm). Flight conditions are given at 42,000 ft (12,800 m) and Mach 2.5 flight. This corresponds to a dynamic head of 1557 psf and inlet recovery, etar, of 0.869 Mil Std. This corresponds to a flight air velocity of 738 m/s, or 1650 mph.

The diffuser itself is a simple body of revolution. The inlet is sized to provide a maximum engine corrected airflow at the assumed engine design conditions. The maximum diffuser throat Mach is 0.786, which corresponds roughly to the throat conditions of an external compression inlet at its maximum corrected flow point, or a mixed compression inlet with a terminal normal shock with approach of Mach of 1.3.

The subsonic diffuser line is a simple spline fit providing a modest divergence half angle of 6 degrees. The equation of the spline is (in inches):

$$r(x) = -0.00034x^3 + 0.012665x^2 + 3.38342$$

The engine spinner is a simple 2:1 ellipse:

$$\left(\frac{x - 33.3}{8.4}\right)^2 + \left(\frac{r - 0}{4.2}\right)^2 = 1$$

Both of the above equations are in inches, however, this report will be in MKS units. The diffuser and spinner shapes shown in Figures 1 and 2 are generated from the above equations. The diffuser ends at the air valve.

A summary of the design conditions in the ram RDE diffuser is shown in Table 1, assuming isentropic deceleration through the supersonic inlet and through the diffuser.

APPROACH

The approach taken in this report is to separate out the diffuser from the combustion chamber and supersonic inlet. Perturbations in the flow from the detonation wave are forced as a pressure perturbation at the exhaust plane of the diffuser. The pressure response through the diffuser is then examined, especially at the diffuser entrance throat, or intake.

To get an accurate representation of the pressure forcing at the exhaust plane, we compute two-dimensional RDE simulations with the geometry and conditions used for this particular ram RDE. That is, the inner and outer diameters are 213 mm and 305 mm respectively, and the feed plenum total pressure and temperature are 2.845 atm and 473 K. We use the solution procedure with a feed plenum and simple

discrete injector air-valve geometry. We have done many simulations of this type [9,10], and the procedure for computing these solutions has been streamlined to a large degree. Stoichiometric ethylene-air is used for the working mixture [11]. The RDE solution procedure assumes a perfectly premixed mixture entering the combustion chamber. The inflow boundary is set to represent the ideal diffuser exhaust. The RDE exhaust boundary is set at free-stream conditions (0.17 atm), resulting in a supersonic outflow. Figure 3 shows a representative solution with the simulation conditions and geometry specified. The two-dimensional simulation is unrolled such that x is the azimuthal direction and y is the axial direction. The features of the typical RDE result have been explained in several papers [12-14]. Both single- and dual-shock operation are computed due to the size of the RDE compared with current laboratory experiments.

Eight separate simulations of this basic RDE are done for this study. Besides single- and dual-shock operation, the only difference between them is the air-valve area ratio (or injection area ratio in previous studies). Since it is a two-dimensional solution, the air-valve is simulated by a number of 2d slot injectors, with the area ratio between the total throat area of all the injectors and the RDE cross sectional area ranging from 0.3 to 0.6. This range corresponds to what is typically seen in experiments and simulations and what values are needed to obtain pressure gain combustion. The global operating conditions for each of these cases are given in Table 2.

The location for the pressure taps are given in Figure 3. The pressure response at two different pressure taps in the feed plenum is given in Figure 4. Pressure oscillations in the feed plenum are small compared to variations in the combustion chamber, but are still significant. Note that in addition to overpressure, an underpressure is also associated with the oscillations. The small peak in the single-shock operation is due to the reflection of the oblique shock wave. This is only seen in the area ratio 0.3 case with single-shock operation. Also note that the static pressure in Figure 4 is greater on average than the injection static pressure and temperature given in Table 1. This is because some of the detonation pressure rise is transferred via an oblique shock wave into the feed plenum. A result of this is that all of our perturbations typically have a higher pressure on average than what is given in Table 1.

This is incorporated into the boundary condition of the diffuser by looking at a snapshot of an entire axial plane of the solution in the feed plenum, which is representative of the exit plane of the diffuser. We choose the same axial location as the first pressure tap, 60 mm from the combustion chamber. The pressure at this plane is shown for all four area-ratios in Figure 5, and the velocity for all the cases is given in Figure 6. The numerous sharp peaks in the profile (especially noticeable for the area ratio of 0.6) are due to the discrete injectors in the air-valve. For the lowest area ratio (0.3) under single-shock operation, the reflected wave can be seen as a broad pressure rise centered near $\theta = 0$ or 2π. Also note that as the area ratio is increased, the main pressure spike at the center of the domain sharpens and becomes a well-defined shock wave, due to less interference between the detonation wave and the upstream conditions. The overall pressure ratio between maximum and minimum pressure in the feed plenum ranged from 1.28 ($a = 0.3$) to 1.96 ($a = 0.6$). Discussion about how this corresponds to the diffuser simulations is given in the next section.

DIFFUSER COMPUTATIONS

The basic diffuser geometry is given by equations 1 and 2. The diffuser is 33.3 inches long (845.82 mm), and has a throat diameter of 6.767 in (171.9 mm). We create an unstructured mesh of tetrahedrals to represent the diffuser using gmesh [15] and a resolution of 0.05 in (1.27 mm). For the baseline diffuser (with no longitudinal vanes) this results in a mesh with 5.69 million points and 31.8 million cells. A representative mesh is given in Figure 7.

The Propel code is used for these computations, which has been used in previous work for RDEs [16] and jet-noise simulations [17]. For the simulations, we use the Propel FEM-FCT solver for an ideal,

constant specific heat gas. The working fluid for the simulations is air with $\gamma = 1.4$ and $R = 287$ kJ/kg K. Because the diffuser handles only air with no reactions at low Mach number, this approximation is excellent. The FEM-FCT solver uses an Element-Based Taylor-Galerkin reconstruction of the conservation equations with synchronized density-energy limiting.

The inflow is a subsonic characteristic boundary treatment. The four incoming characteristics (one acoustic wave and three entropy-related characteristics) are specified using the Station 2 conditions, while the remaining acoustic wave is extrapolated from the interior. The exit flow also uses a characteristic treatment, where one acoustic wave is specified from the exit boundary conditions and four characteristics are extrapolated from the interior. The exhaust boundary conditions are spatially varying and time-dependent and are based on the feed-plenum plane results from the RDE simulations (Figs. 5 and 6). This solution has azimuthal variation and no radial variation. The whole exit forcing solution is rotated azimuthally at the average velocity of the detonation wave from the corresponding RDE simulation, giving the forcing a dominant frequency set by the detonation wave in the RDE.

Diffuser Simulations without Exit Forcing

The first diffuser results we computed are for the non-perturbed case. We set the inflow of the diffuser with conditions from station 1.2 (Table 1), and set the exit pressure to the conditions at Station 3. This computation was done to ensure that we recover the ideal solution without forcing. The result for the baseline case is shown in Figure 8. The flow is nearly one-dimensional and decelerates as the diffuser widens, and then accelerates again as the cross-sectional area decreases due to the spinner. Pressure taps are taken for several radii at the diffuser throat (intake) and also along the wall. The steady-state pressures at the pressure taps for the no-forcing case are given in Figure 9. The pressure at the exit matches the predicted value of 2.58 atm accurately.

Diffuser Simulations with Exit Forcing

As we include the exhaust forcing, the solution becomes fundamentally different, as shown in Figure 10. This figure shows the instantaneous pressure with exit forcing from the RDE solution with area ratios of 0.3 and 0.6 in single- and dual-shock operation. The addition of exit forcing creates a shock wave that propagates upstream against the main flow. There is both an azimuthal and axial component of the shock wave. The shock wave expands (and weakens) around the spinner, and continues to propagate upstream towards the diffuser throat. The lower area ratio solutions (Figs. 10a and 10b) are considerably more noisy than the higher area ratio because the pressure forcing is much more poorly defined for the lower area ratio than the higher area ratios.

Figure 11 and 12 show the intake solution at 8 different time snapshots during 1 cycle for the low area ratio case under single-shock and dual-shock operation. Both of these time series demonstrate that for these cases, the pressure response essentially rotates as a solid body around the axis of rotation. This is expected since the exit forcing is essentially a solid body rotation as well, and there is no azimuthal variation in the geometry to break the solid body rotation. Because of this, the pressure perturbation must vanish as you approach the centerline.

Figure 13 shows the pressure history at the pressure taps located at the diffuser throat and along the axial wall for an area ratio of 0.3, single-shock operation. At the diffuser intake, it is clear that the pressure perturbation uniformly increases from almost 0 at the centerline to a large range (2.58 atm – 3.08 atm) at the outer wall. The pressure taps along the wall are much more difficult to interpret in Figure 13, therefore we broke them into individual pressure traces in Figure 14. The signal shape changes quite dramatically along the axis of the diffuser, but the overall pressure change remains very similar. The dominant frequency for all these cases is the forcing frequency specified at the exhaust boundary. The changes in the shape of the signal correspond to shifting energy between the different harmonics due to the diffuser geometry. There is only a small amount of damping of the signal between the exit and intake for this case.

To ensure that the results were grid independent, case 1 was rerun with double the resolution (from 0.05 inch to 0.025 inch resolution). This increased the number of points from 5.7 million to 54.0 million, and the number of tetrahedral cells from 31.8 million to 320.7 million. The 0.05 in resolution took 5.4 hours to run 0.02 s of physical time on 32 GPUs, whereas the 0.025 in resolution took 54.4 hours to run 0.02 s of physical time on 64 GPUs. Three resolutions are shown in Figure 15 for the pressure tap near the diffuser intake at the wall. The lower resolution case with 0.10 inch resolution is shown for comparison. All three resolutions resolve the basic shape of the pressure response, however, the lowest resolution shows considerable diffusion and underpredicts the smaller peak substantially. The 0.05 inch and 0.025 inch cases are very similar, and both of the pressure spikes are resolved correctly. The error in the minimum and maximum values for the pressure between the two resolutions is 0.3% and 0.1% respectively. All of the remaining cases were run with the 0.05 inch resolution.

Effect of RDE Area Ratio

In addition to the area ratio of 0.3, we are also interested in area ratios up to 0.6, with forcing indicated in Figs. 5 and 6. Because of this, a total of 8 simulations where run with 4 different area ratios and single- and dual-shock operation. The forcing given in Figs. 5 and 6 results in a time-history at the wall near the exhaust plane given in Figure 16. This looks as we would expect, and very close to the exit plane forcing seen in Figure 5.

Figure 17 is the pressure response at the diffuser intake, and is much more interesting. Focusing first on Fig. 17a, notice that although all of the perturbations are lower than the exhaust forcing at the exit of the diffuser, the higher area ratio cases have a much stronger perturbation than the lower area ratio cases. However, for the dual-shock operation, the perturbations at the inlet have all become very similar, regardless of the exhaust area ratio.

Figure 18 better illustrates this by comparing the percent variation at different stations. The percent variation is simply calculated as:

$$\% \text{ Variation} = \frac{(P_{max} - P_{min})}{(P_{max} + P_{min})/2}$$

Stations 1-7 are at the intake plane, and correspond to the different radii in Figure 13a (Station 1 is at the centerline). Stations 7-13 are along the wall at different axial locations, as shown in Figs. 13b and 14. The spread of variation between the low area ratio and high area ratios in the single-shock operation is strongly evident throughout the diffuser. Note that for the low area ratio, there is almost no damping between the exhaust plane and the intake of the diffuser. This is due to the broadness of the lower area ratio pressure forcing (shown in Fig. 5a). The broader the pressure spike, the less it can be effectively damped as it propagates upstream towards the intake.

The more interesting result in Figure 18 is for the dual-shock operation. Unlike the single shock operation, in dual-shock operation, all of the different area ratios result in a very similar perturbation at the intake, as suggested by Figure 17. The reasoning is similar to what we noted above. Comparing the pressure forcing between the single- and dual-shocks in Figure 5, all cases (except for the lowest area ratio) show a much narrower pressure peak for the dual-shock, although the magnitude of the pressure peak is very similar. This sharper pressure spike results in more decay of the wave as it travels towards the intake of the diffuser. The collapse of the pressure perturbation is fairly rapid, and is most like caused by the expansion of the wave around the spinner for the dual-shock cases.

This suggests that under some circumstances, the high area ratios should not significantly affect the amount of pressure perturbation that is seen at the intake. Since the higher area ratios are required for

actual pressure gain combustion, this is a positive result. More guidance is needed on when to expect the area ratio to make a difference. Guidance is also needed on what strategies may reduce the overall perturbation that is seen.

RELEVANCE FOR INLET PERFORMANCE AND OPERABILITY

Almost all supersonic inlets have an inherent stability range which is a function of the freestream conditions, the inlet design and the downstream conditions. Significant variations in the downstream airflow or pressure can result in inlet performance degradation or stability issues. The average RDE airflow and pressure requirements can be relatively easily accommodated when designing the inlet. The dynamic pressure fluctuations generated by the current RDE designs create a unique compatibility challenge to the inlet designer.

The high frequency (i.e. pressure f> 1,000 Hz) rotating, dynamic oscillation imposed by the RDE on the inlet are unique. Since the pressure oscillations only effect a small portion of the inlet and they are very transient, it is conceivable that the inlet flow will not be able to react to the pulses as it would a planar pulse. Further research is necessary to quantify the effect of this dynamic disturbance on the inlet flowfield. In the interim, to insure safe inlet operation, the disturbance must be handled as if it were a low frequency planar pulse. Supersonic inlets have repeatedly shown that the inlet will respond to such disturbances as if the disturbance were steady-state. Therefore, to insure stable inlet operation, sufficient margin would have to be designed into the inlet's operating map to accommodate the dynamic disturbance. This would result in increased inlet margins being required, which in turn would decrease the average inlet pressure recovery.

Further research is required to: a) define how the supersonic inlet will respond to the high frequency dynamic pressure disturbance currently imposed by the RDE and 2) investigate methods of mitigating the magnitude of the pressure disturbance that the RDE generates.

SUMMARY

This report has focused on dynamic simulations of a representative ram RDE subsonic diffuser to study ram RDE compatibility with a supersonic inlet. Of particular interest is the propagation of pressure perturbations due to the detonation waves in the RDE combustion chamber. Simulations were completed using a notional diffuser for a ram RDE device operating at 42,000 ft and Mach 2.5. A previous RDE code was used to provide an exhaust forcing function assuming a slot injector plate. A total of 8 different exhaust forcing functions were used, representing RDE air-valve area ratios between 0.3 and 0.6 in single and dual shock operation. Simulations were then completed for the diffuser with the Propel code for each of these exhaust forcing functions.

Analysis indicates that the amount of pressure variation seen near the inlet is very sensitive to the shape of the forcing function. The broad pressure rise of the lower area ratios tend to remain intact through the diffuser to the intake with minimal dissipation, while the sharper pressure peak of the higher area ratios tend to be dissipated to a larger degree. For single-shock operation, the amount of pressure variation at the intake varies from 20.5% (area ratio of 0.3) to 39.1% (a=0.6). Dual-shock operation further sharpens the peak of the forcing function. For dual-shock operation, the amount of pressure variation at the intake varies from 21.0% (a=0.3) to 21.9% (a=0.6) for the different area ratios. The last result is encouraging, because the higher area ratios and larger mass-flow rates will most likely operate with multiple shocks, or detonation waves.

Further work is required to determine the response of the inlet to these disturbances and ways to further mitigate the pressure perturbations through the geometry of the diffuser, while maintaining an efficient diffuser design.

ACKNOWLEDGEMENT

This work was sponsored by the Office of Naval Research.

REFERENCES

1. Nordeen, C.A., Schwer, D.A., Corrigan, A. and Cetegen, B., "Radial Effects on Rotating Detonation Engine Swirl," AIAA Paper 2015-3781, AIAA Prop & Energy 2015, Orlando, FL, July 27-29, 2015.

2. Rankin, B. A., Hoke, J., and Schauer, F., "Periodic Exhaust Flow through a Converging-Diverging Nozzle Downstream of a Rotating Detonation Engine," AIAA Paper 2014-1015, AIAA SciTech 2014, Washington, DC, 2014.

3. Walsh, P.P., and Fletcher, P., *Gas Turbine Performance*, 2nd edition, Blackwell Publishing, pp. 255, 617-619.

4. Heiser, W.H., and Pratt, D.T., "Thermodynamic Cycle Analysis of Pulse Detonation Engines," *J Propulsion Power*, Vol. 18, No. 1, p. 68, 2002.

5. Braun, E.M., Lu, F.K., Wilson, D.R., and Camberos, J.A., "Airbreathing Rotating Detonation Wave Engine Cycle Analysis," *Aerosp Sci Technol*, Vol. 27, No. 1, pp. 1-8, 2013.

6. Paxson, D.E., and Kaemming, T.A., "Influence of Unsteadiness on the Analysis of Pressure Gain Combustion Devices," *J Propulsion Power*, Vol. 30, pp. 377-383, 2014.

7. Schwer, D.A., and Kailasanath, K., "Thermodynamic Properties of a Rotating Detonation Engine," 7th US National Combustion Meeting, Atlanta, GA, March 20-23, 2011.

8. Nordeen, C.A., Schwer, D.A., Schauer, F., Hoke, J., Barber, T., and Cetegen, B., "Thermodynamic Model of a Rotating Detonation Engine," *Combustion, Explosion, and Shock Waves*, Vol. 50, No. 5, p. 568, 2014.

9. Schwer, D.A., and Kailasanath, K., "Effect of Inlet on Fill Region and Performance of Rotating Detonation Engines," AIAA Paper 2011-6044, 47th AIAA/ASME/SAE/ASEE Joint Propulsion Conference, 2011.

10. Schwer, D.A., and Kailasanath, K., "Feedback into Mixture Plenums in Rotating Detonation Engines," AIAA Paper 2012-0617, 50th AIAA Aerospace Sciences Meeting, 2012.

11. Schwer, D.A., and Kailasanath, K. "Fluid Dynamics of Rotating Detonation Engines with Hydrogen and Hydrocarbon Fuels," *Proc Combust Inst*, Vol. 34, p. 1991, 2013.

12. Hishida, M., Fujiwara, T., and Wolanski, P., "Fundamentals of rotating detonation engines," *Shock Waves*, Vol. 19, No. 1, pp. 1-10, 2009.

13. Schwer, D.A. and Kailasanath, K., "Numerical investigation of the physics of rotating detonation engines," *Proc Combust Inst*, Vol. 33, p. 2195, 2011.

14. Zhou, R., Wang, J.-P., "Numerical investigation of flow particle paths and thermodynamic performance of continuously rotating detonation engines," *Combust Flame*, Vol. 159, No. 12, pp. 3632-3645, 2012.

15. Geuzaine, C. and Remacle, J.-F., "Gmsh: a three-dimensional finite element mesh generator with built-in pre- and post-processing facilities," *International Journal for Numerical Methods in Engineering*, Vol. 79, No. 11, pp. 1309-1331, 2009.

16. Schwer, D.A., Corrigan, A., and Kailasanath, K., "Towards Efficient, Unsteady, Three-Dimensional Rotating Detonation Engine Simulations," AIAA Paper 2014-1014, AIAA SciTech 2014, National Harbor, MD, Jan 13-17, 2014.

17. Liu, J., Corrigan, A., Kailasanath, K., Ramamurti, R., Heeb, N., Mundary, D., and Gutmark, E. "Impact of Deck and Jet Blast Deflector on the Flow and Acoustic Properties of Imperfectly Expanded Surpersonic Jets," AIAA Paper 2013-0323, 51st AIAA Aerospace Sciences Meeting, 2013.

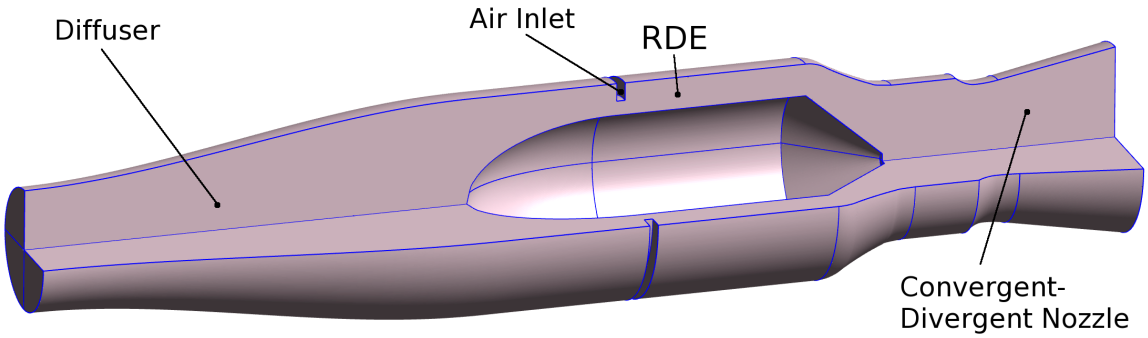

Figure 1 — A notional ram RDE engine

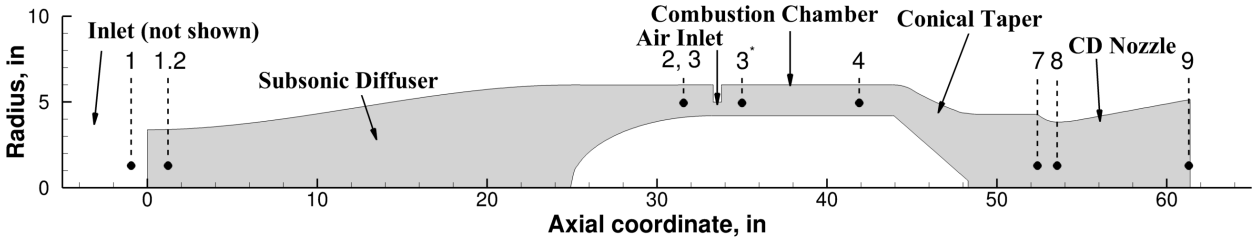

Figure 2 — Ram RDE cross-section with thermodynamic stations labeled on it

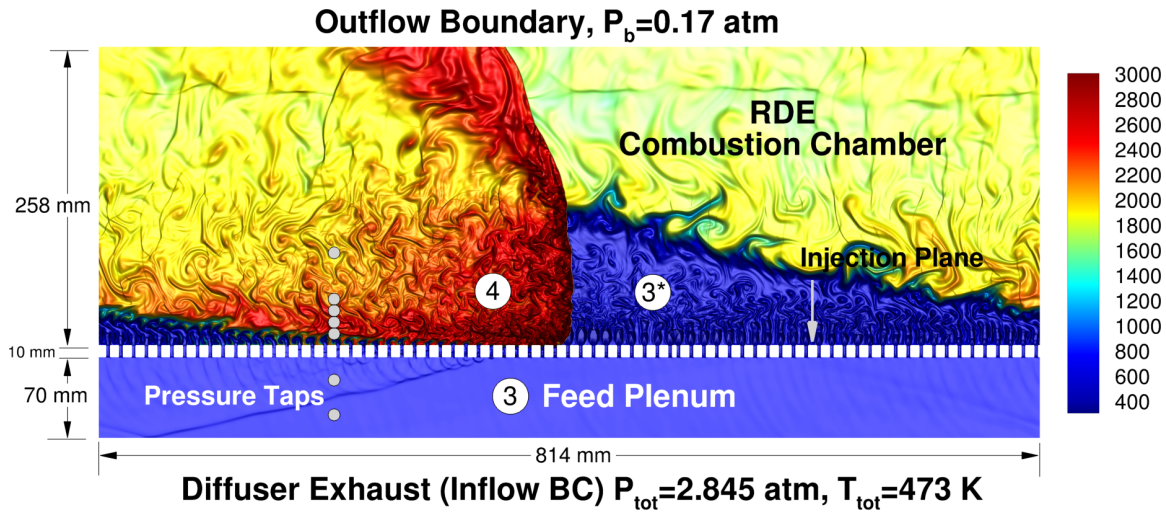

(a) single shock operation

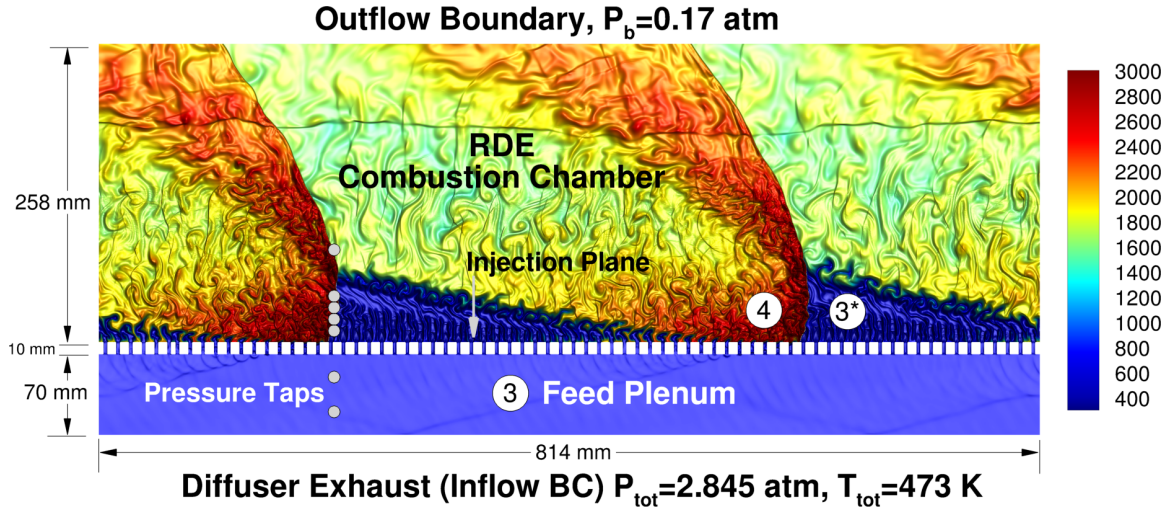

(b) dual shock operation

Figure 3 — RDE Geometry and conditions used for solution. Thermodynamic stations for 3, 3*, and 4 are also shown on the plot.

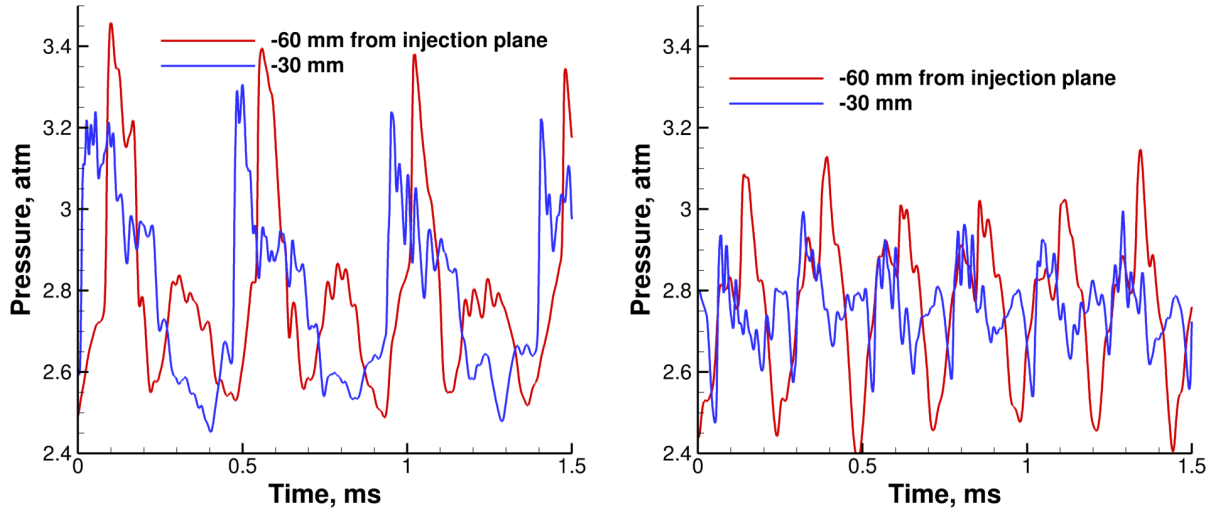

(a) single shock (b) dual shock

Figure 4 — Pressure response in the feed plenum below the air-valve

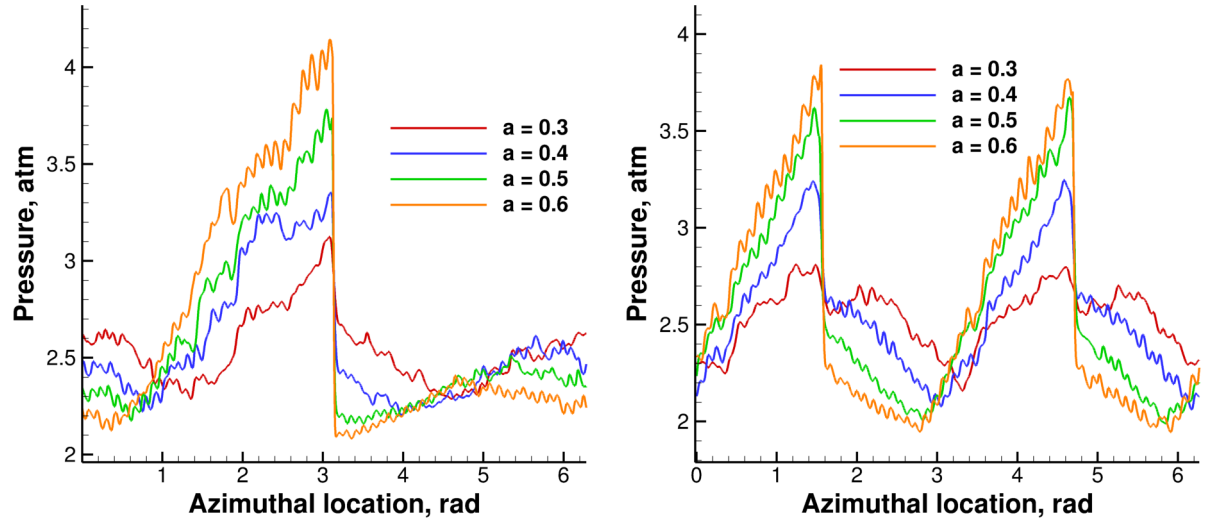

(a) single shock (b) dual shock

Figure 5 — Pressure response in the feed plenum for different area ratios

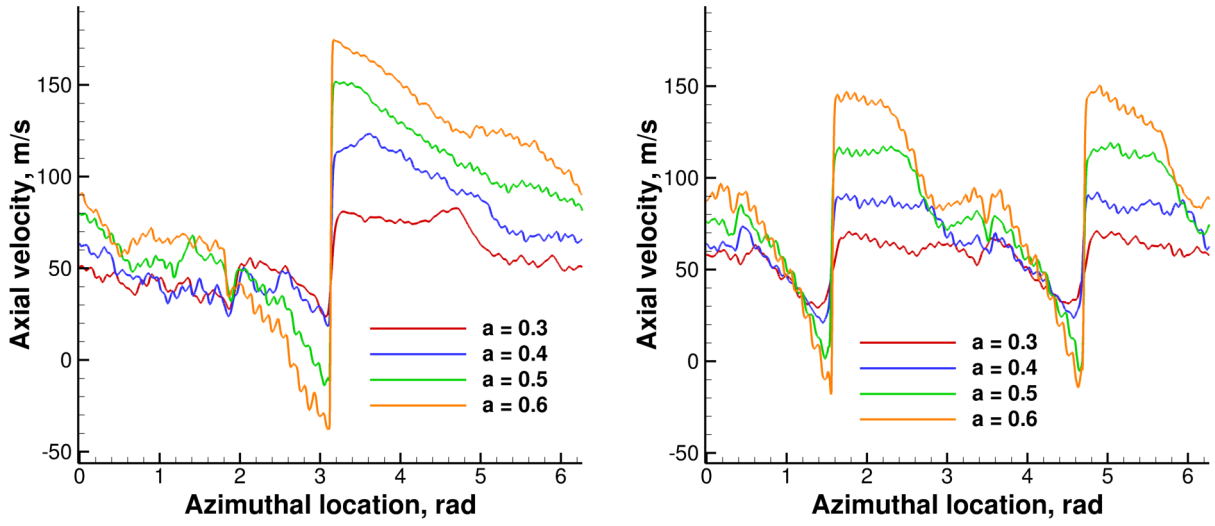

(a) single shock (b) dual shock

Figure 6 — Axial velocity response in the feed plenum for different area ratios

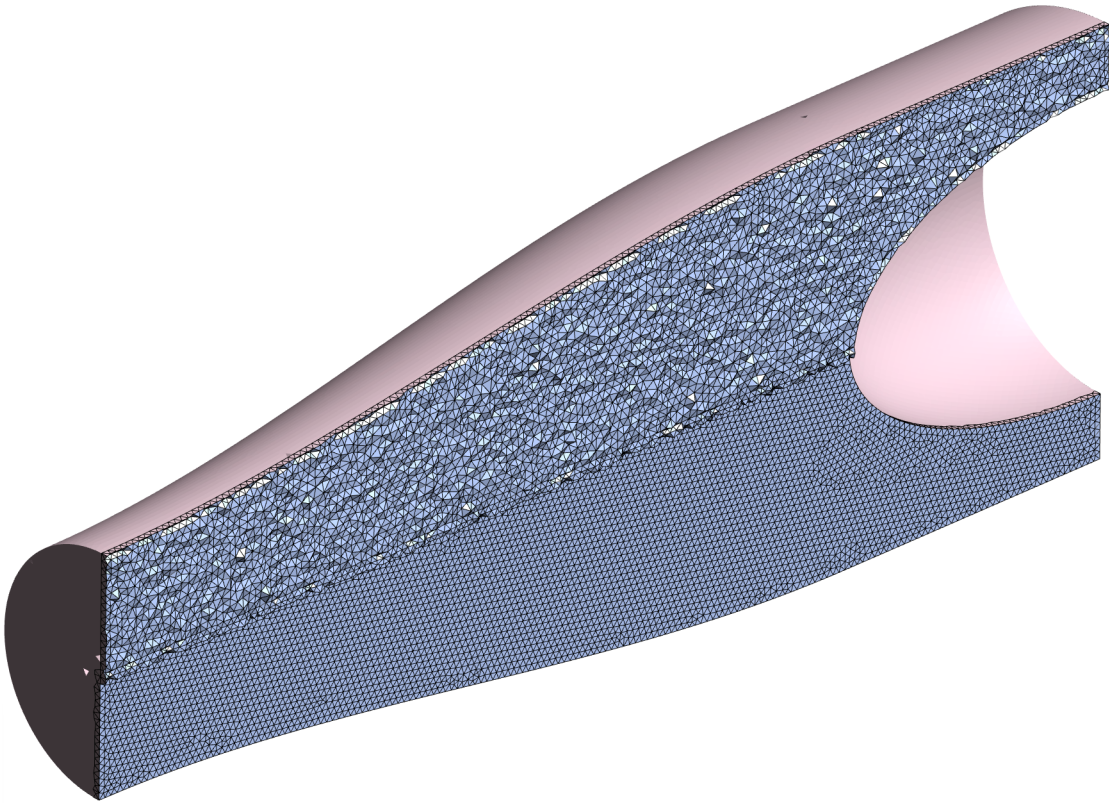

Figure 7 — Representative mesh showing inflow and outflow of the diffuser. This mesh has a resolution of 0.2 in, and is coarser than the meshes used for the simulations.

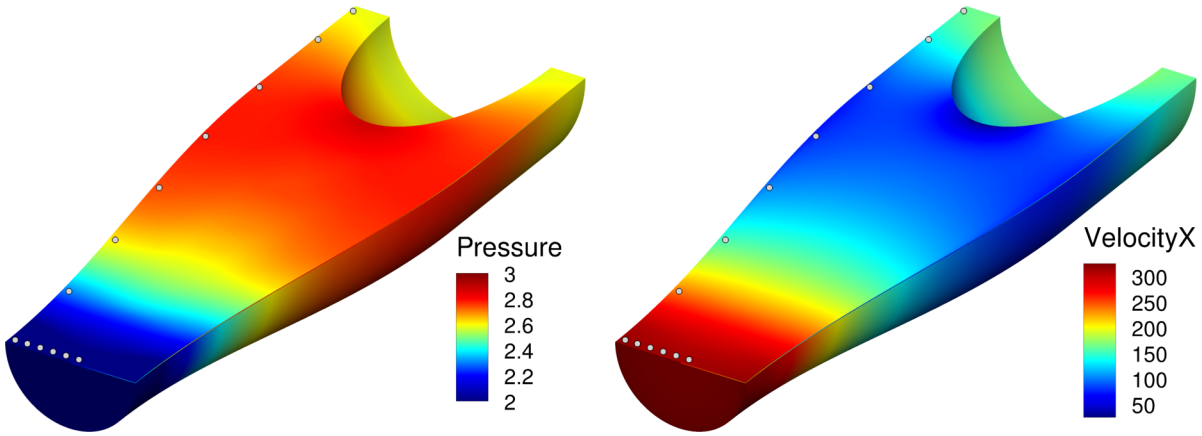

(a) Pressure (b) Axial Velocity

Figure 8 — Pressure and velocity for baseline geometry and no exhaust forcing. Circles indicate approximate location of pressure taps at diffuser throat and wall.

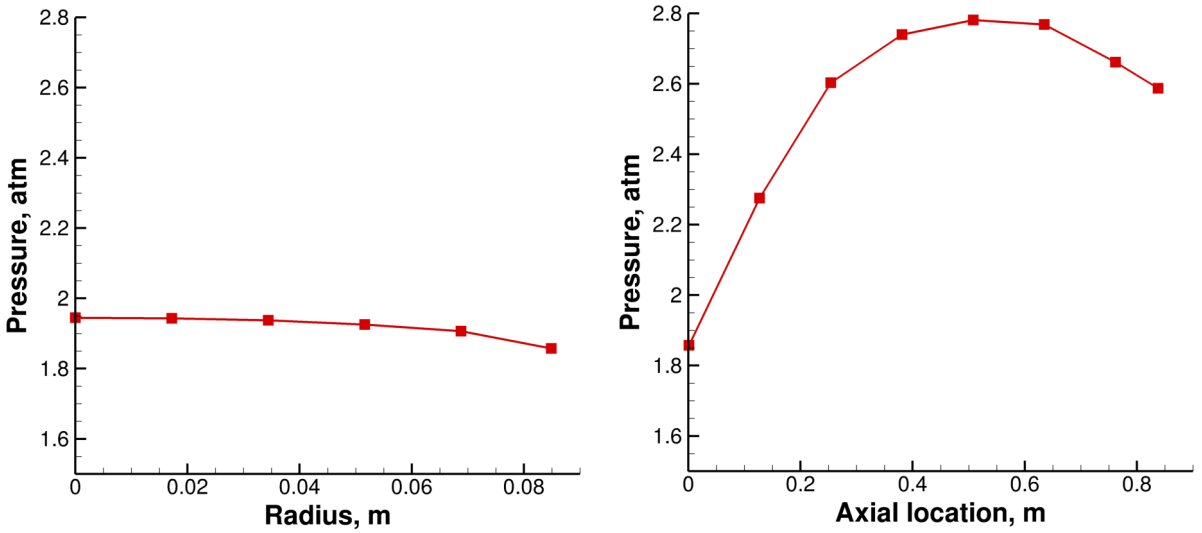

(a) diffuser throat (b) axial wall

Figure 9 — Pressure at pressure taps for cases with no forcing

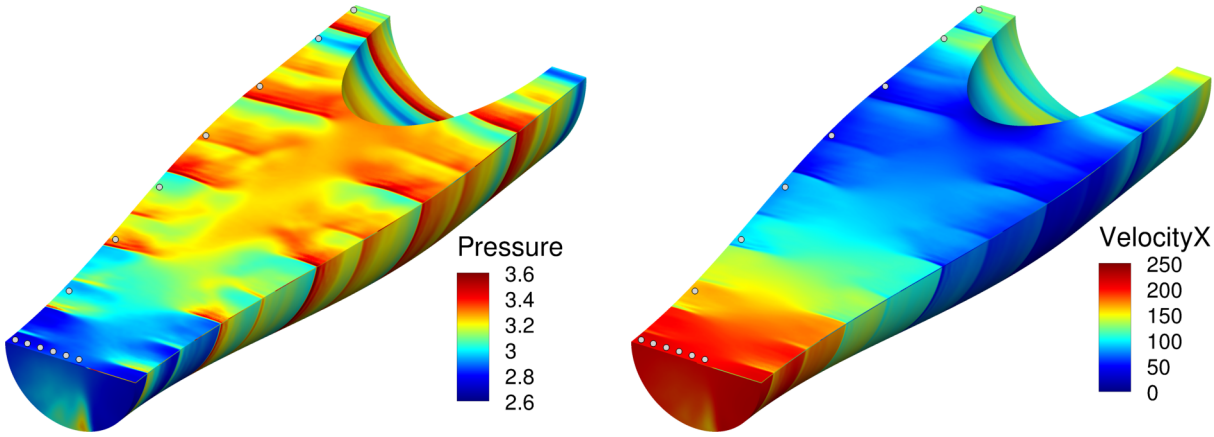

(a) Area ratio of 0.3, single-shock operation

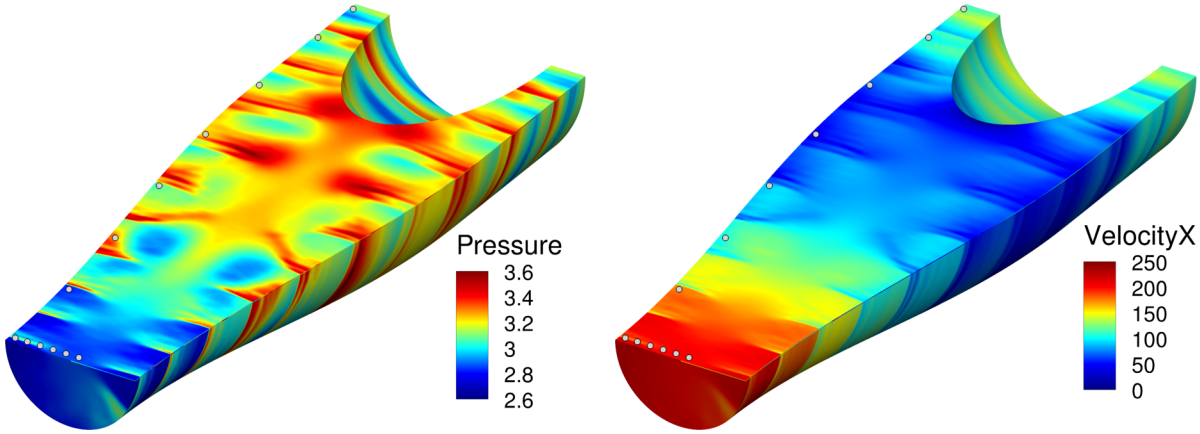

(b) Area ratio of 0.3, dual-shock operation

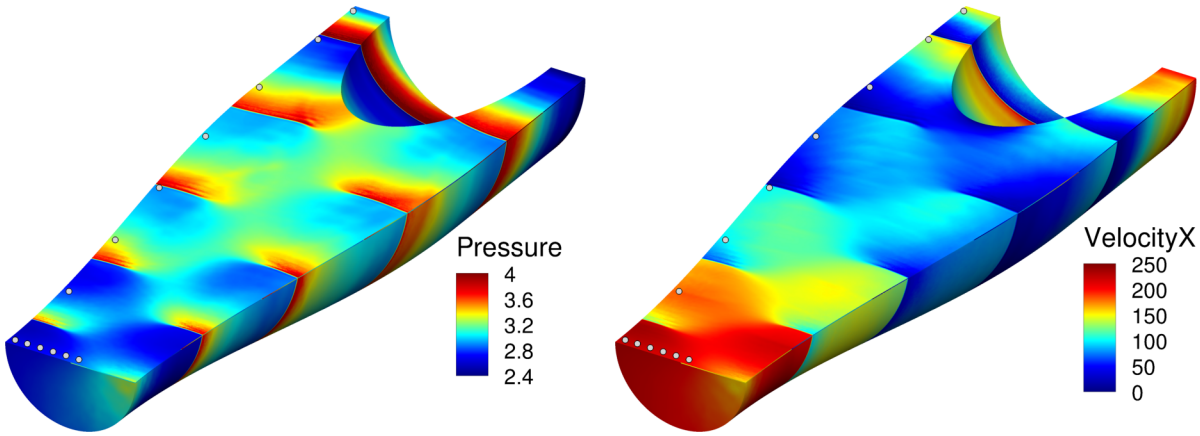

(c) Area ratio of 0.6, single-shock operation

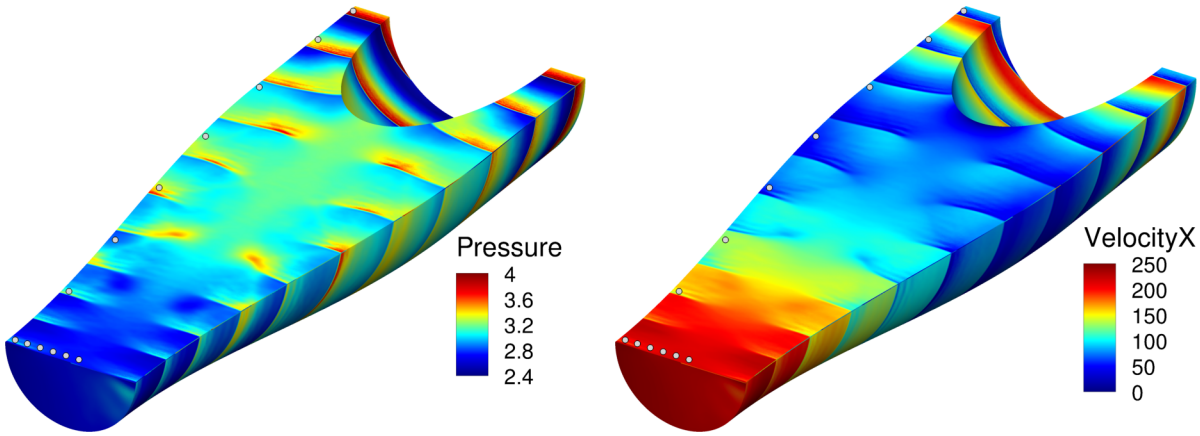

(d) Area ratio of 0.6, dual-shock operation

Figure 10 — Pressure and axial velocity for a snapshot for the baseline geometry and exhaust forcing from RDE

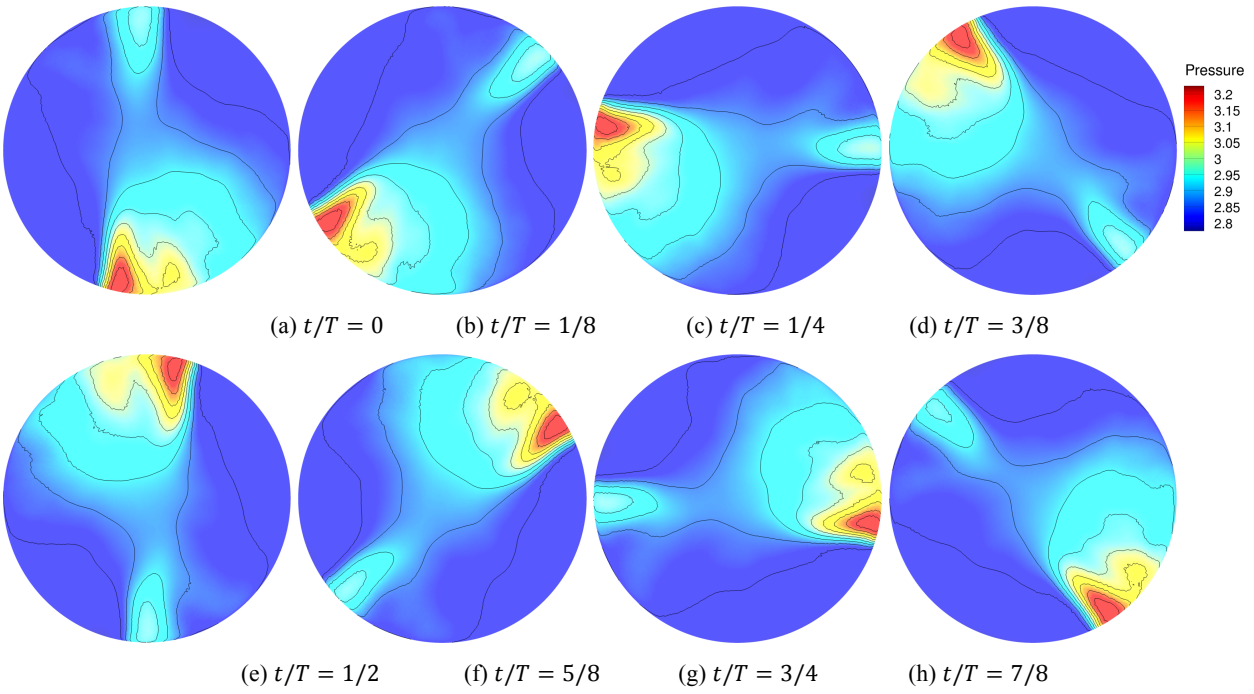

Figure 11 — Snapshots of the intake pressure over one main period. Area ratio is 0.3, single-wave solution. T=462 μs. Pressure range = 2.71 atm – 3.23 atm.

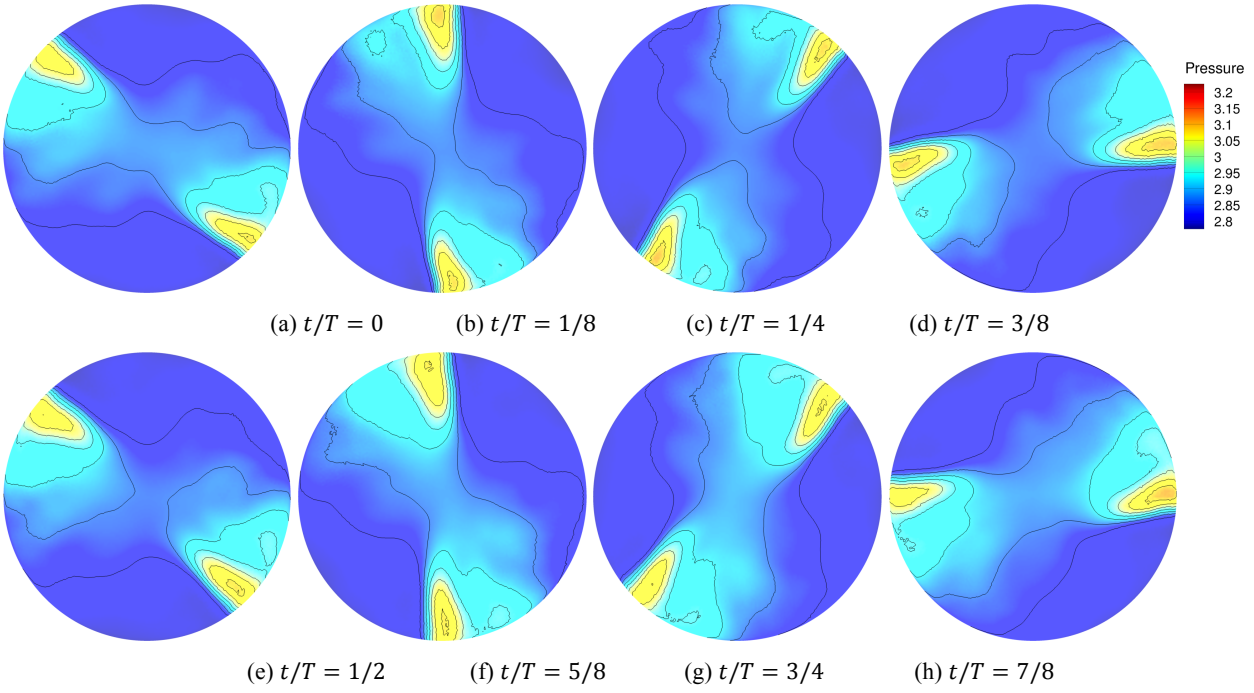

Figure 12 — Snapshots of the intake pressure over one main period. Area ratio is 0.3, dual-wave solution. T=466 μs. Pressure range = 2.70 atm - 3.11 atm.

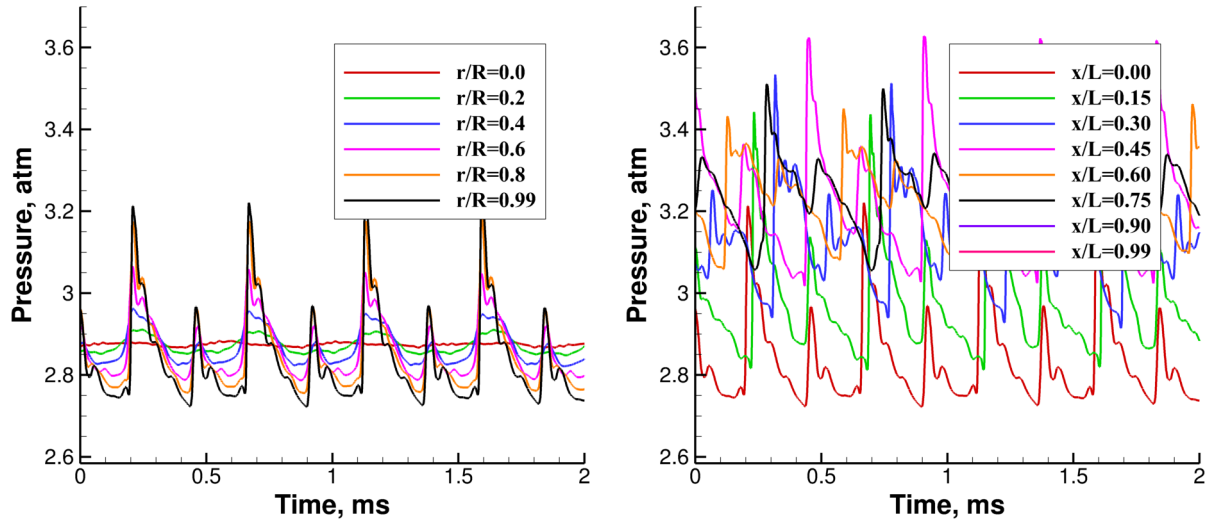

(a) diffuser throat (b) axial wall

Figure 13 — Radial pressure taps at diffuser throat (left) and pressure taps along the wall (right) for the diffuser with exhaust forcing. Baseline geometry and area ratio of 0.3.

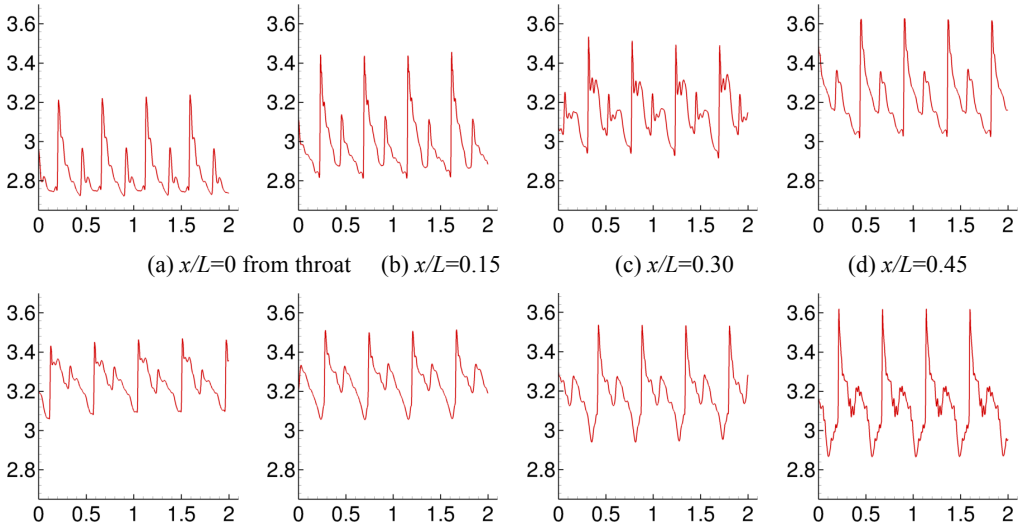

(a) x/L=0 from throat (b) x/L=0.15 (c) x/L=0.30 (d) x/L=0.45

(e) x/L=0.60 (f) x/L=0.75 (g) x/L=0.90 (h) x/L=0.99

Figure 14 — Pressure (atm) vs. Time (ms) at pressure taps along the wall for diffuser with exhaust forcing. Baseline geometry and area ratio of 0.3.

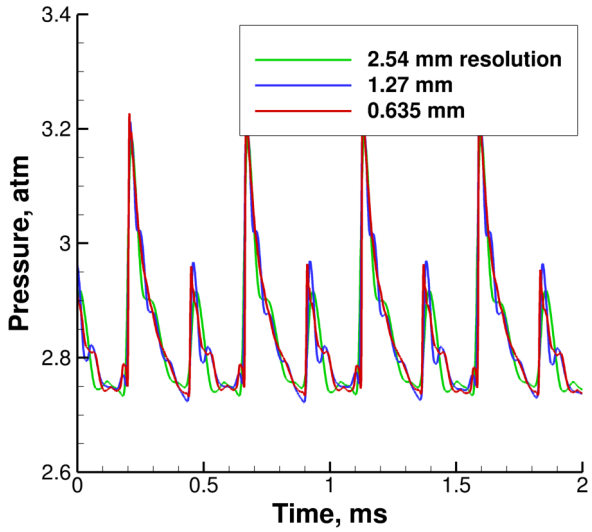

Figure 15 — Comparison of wall pressure tap at diffuser intake at different grid resolutions. Baseline geometry with area ratio of 0.3.

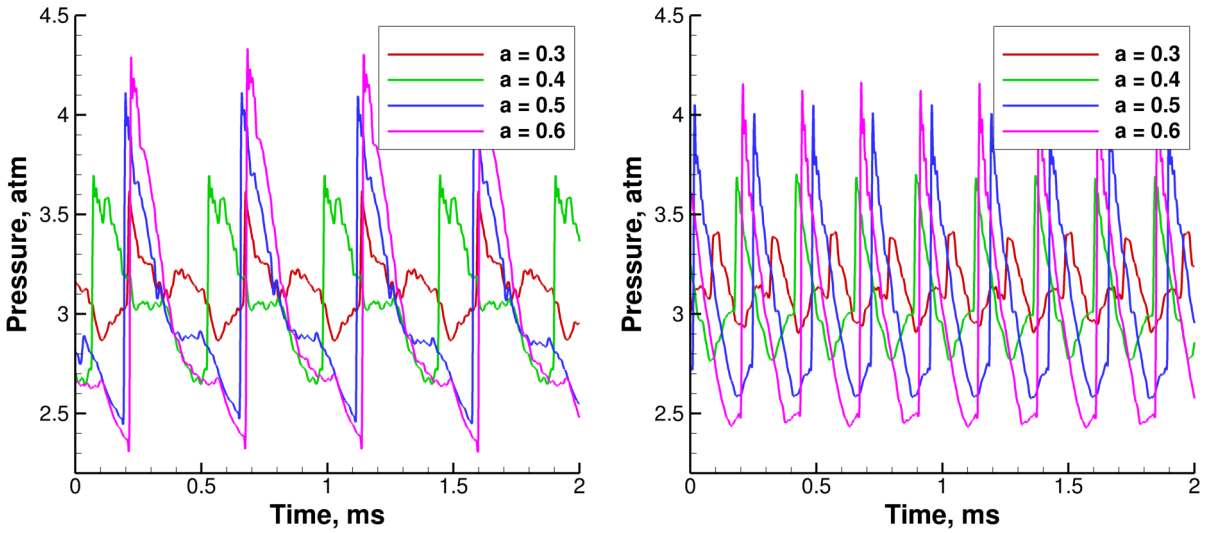

(a) single shock (b) dual shock

Figure 16 — Comparison of wall pressure tap near exit of diffuser for different area ratio RDEs.

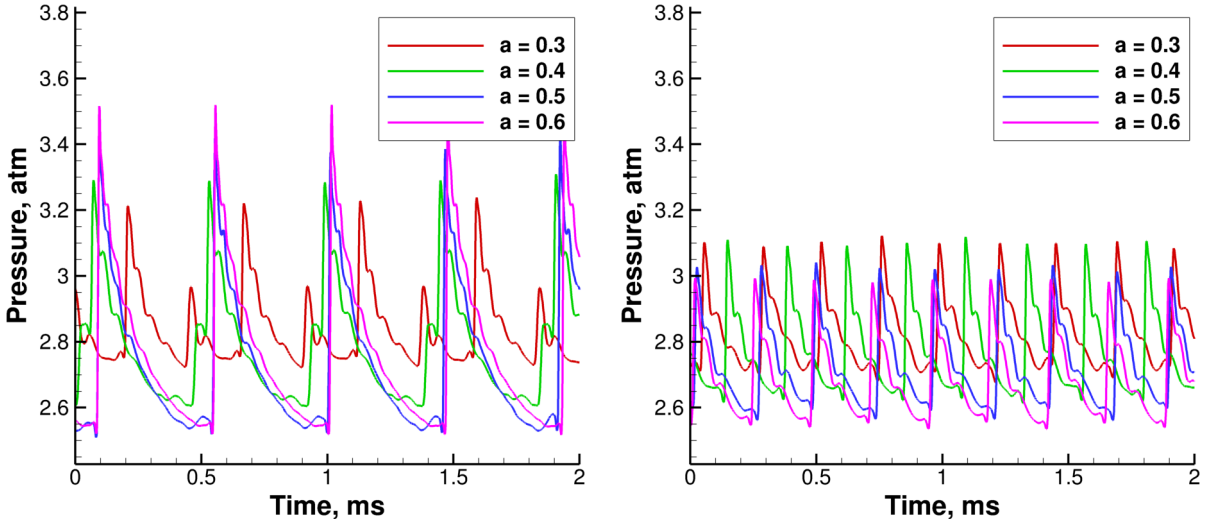

(a) single shock (b) dual shock

Figure 17 — Comparison of wall pressure tap near throat of diffuser for different area ratio RDEs. Baseline diffuser.

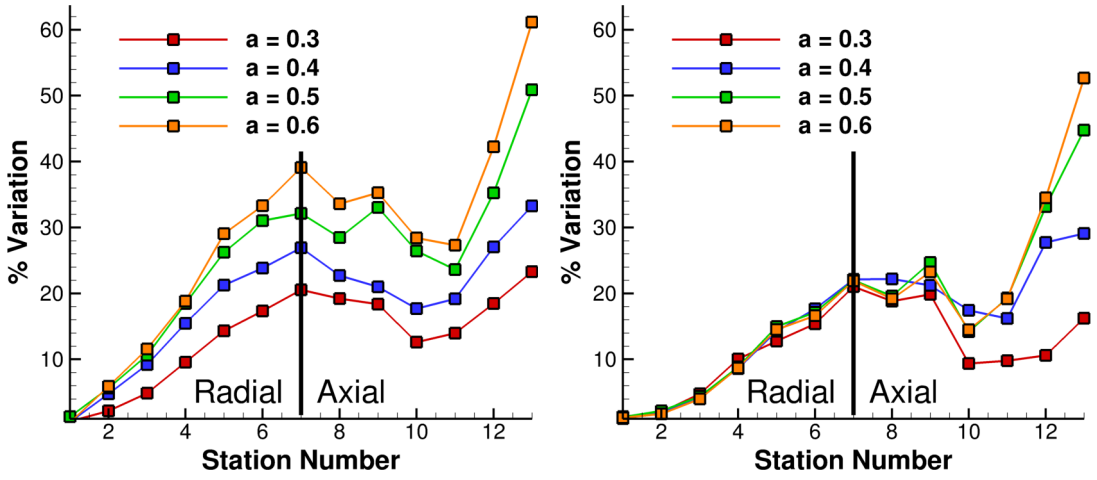

(a) single shock (b) dual shock

Figure 18 — Variation in the pressure with respect to the mean local pressure at the different stations in the diffuser. Stations 1-7 are radial at inlet throat from the centerline out to the wall. Stations 7-13 are along the wall from the throat to the exhaust plane. Baseline diffuser.

Table 1 — Ideal conditions ahead of and through the diffuser

Station	Description	Mach	Pressure (atm)	Temperature (K)	P_{tot} (atm)	T_{tot} (K)
∞	Free stream	2.5	0.17	216	2.905	486
1	Supersonic Inlet	1.3	1.048	363	2.905	486
1.2	Diffuser Throat	0.786	1.892	433	2.845	486
2,3	Diffuser Exhaust	0.375	2.581	473	2.845	486

Table 2 — Operating conditions of the RDE used for diffuser exhaust forcing

Air-Inlet Area Ratio	Mass flow rate (kg/s)	Force (N)	Isp_f (s)	Det. Wave Velocity (m/s)	Plenum Pressure (atm)
0.3-single	4.16	5850	2250	1764	2.28 — 3.12
0.4	5.01	7200	2300	1776	2.21 — 3.35
0.5	5.77	8370	2320	1772	2.16 — 3.78
0.6	6.44	9370	2330	1767	2.08 — 4.14
0.3-dual	4.24	6000	2260	1745	2.16 — 2.81
0.4	5.06	7290	2300	1716	2.06 — 3.25
0.5	5.74	8320	2320	1730	1.99 — 3.67
0.6	6.32	9190	2330	1734	1.94 — 3.84